Article ID: 1000-7032(2011)06-0542-08

Influence of Particle's Deformation on The Optical Properties of Silica Opal Photonic Crystals

CUI Nai-di[1,2], LIANG Jing-qiu[1], LIANG Zhong-zhu[1], ZHOU Jian-wei[1,2], WANG Wei-biao[1*]

(1. *State Key Laboratory of Applied Optics, Changchun Institute of Optics, Fine Mechanics and Physics, Chinese Academy of Sciences, Changchun* 130033, *China*;
2. *Graduate School of the Chinese Academy of Sciences, Beijing* 100039, *China*)

Abstract: The opal photonic crystals were fabricated with silica colloidal particles. These opal photonic crystal samples were annealed at 150, 300, 450 ℃ separately. For the photonic crystals annealed at 450 ℃, the central wavelength of photonic band gap(PBG) was measured at 572.5 nm, which was greatly different from the calculated result at 605 nm. In addition, the samples showed a blue shift for 22.5 nm and a reduction of the photonic band gap width upon increasing the annealing temperature. The shrink and deformation of silica colloidal particles were observed by SEM. The influence mechanism of the deformation was analyzed quantitatively, and the theoretical model was amended. The central wavelength of PBG re-calculated with the amended dodecahedron model was 558 nm, which fit the measured result much better than that calculated with the old sphere model. The new dodecahedron model provides a way to analyze the optical properties of the deformed opal PCs in theory, and shall be of significant value on the fabrication and application of photonic crystals devices.

Key words: photonic crystals; self-assembly; photonic band gap
CLC number: O431.1 **PACS:** 42.70.Qs **PACC:** 4270Q; 4225B **Document code:** A

1 Introduction

Photonic crystals (PCs) are ordered nanostructures in which mediums with different dielectric constants [1-2] were arranged periodically. Much scientific and technological attention has been attracted for the unique optical properties of PCs. The dielectric materials in PCs act like the periodical nuclei in crystalline solids. Like the semiconductor, the PCs provide photonic band respect to the electronic band in semiconductor. The PCs can yield a photonic band gap, in which electromagnetic waves with certain frequency are forbidden to propagate. If the electromagnetic waves are forbidden in all the possible direction, the complete PBG is achieved. The phenomenon of photonic band gap can be used to control the flow of light [3-4]. PCs can be used to fabricate optoelectronic devices, such as near-zero threshold lasers [5], waveguides [6], antennas [7], couplers [8], filters [9], which will be of significant value in the future photonic/optical circuits.

For the 1D and 2D PCs, it can be achieved by programmed deposition of different dielectric material layers, holographic exposure, and etching through a mask and some other MEMS technics [10-13]. Some precision machinery methods are the conventional way to fabricate 3D PCs in the microwave and terahertz wave band. However, in near infrared or the visible light wave band, the period of PCs is usually in several hundreds nanometers, which takes great

Received date: 2011-04-25; **Revised date:** 2011-05-15
Foundation item: The works was supported by National Natural Science Foundation of China (60877031)
Biography: CUI Nai-di, born in 1983, male, Heilongjiang Priovince. His work focuose on the design and fabrication of the photonic crystals opt-electronic devices.
E-mail: cunaidi@163.com
*: Corresponding Author; E-mail: wangwbt@126.com

challenges to the precision machinery technics. Thereupon, new methods such as direct writing [14], multi-beam interference [15], and self-assembling [15-17] were proposed. Self-assembly methods are developed as an inexpensive and simple way to fabricate 3D PCs in a large area mimic the opal in nature. Compared with the opal PCs, the inverse opal PCs show a complete photonic band gap (PBG). Using the opal PCs as template, the inverse opal PCs can be fabricated [18-20]. The self-assembly of colloidal crystals can be achieved by gravity sedimentation [21], vertical deposition [22], electrophoresis [23], and spin coating [24] *etc*. Similar to crystal in solid state, the opal PCs fabricated by these methods will bring some kinds of defects inevitably.

Vlasov *et al*. introduced the temperature gradient field, which provides an effective way to decrease the defects of the colloidal crystals [25]. Yan *et al*. fabricated metallic opal PCs by double templating method [26]. The work by Meng *et al*. proposed a new method to fabricate high-quality large-scale inverse opal PCs through controling the temperature, pressure and infrared intensity in 15 to 30 min [27]. Sun *et al*. fabricated non-spherical colloidal crystals by thermo-pressing spherical polymer colloidal crystal chips [28]. These works provide novel ways for the fabrication of the colloidal PCs. In the work of Sun *et al*., because of the thermo-pressing, the deformation of the colloidal particles is observed. Besides, the deformation widely appears in some other works, though many samples were fabricated without heat treatment or pressing [29-30]. The deformation comes from the compression of the internal stress. The internal stress makes the particles arrange closely to each other, which enhances the mechanical strength and density of the opal PCs greatly. Therefore, the deformation of the particles makes it possible to fabricate devices using colloidal PCs. However, little attention has devoted to the application of the deformed PCs. Besides, until recently, there is some lack of knowledge about the influence mechanism of the deformation. In this paper, the silica colloidal crystals are fabricated with vertical deposition, and we focus on the influence of the deformation on the optical properties and photonic band structure.

2　Theoretical Calculation

In calculation, silica colloidal particle is deemed to sphericity (sphere model). The diameter (D) of silica colloidal particle is 275 nm (standard deviation < 5%), and the refractive index (n_s) of silica is 1.45 approximately. The central wavelength of the PBG is calculated with the Bragg's law, and the width of the PBG is calculated with plane wave expansive (PWE) method.

2.1　Bragg's Law

The central wavelength of PBG in face centre cube (FCC) PCs was calculated though a modified form of Bragg's law, which provides a simple relation between the central wavelength (λ), the spacing of (111) domains (d_{nkl}), the effective refractive index (n_{eff}) and the incident angle (θ):

$$\lambda = 2d_{nkl}\sqrt{n_{eff}^2 - \sin^2\theta}, \qquad (1)$$

where $d_{nkl} = 0.816d$, d is the spacing of the adjacent two spheres. The effective refractive index (n_{eff}) is related to the volume fraction (f), the refractive index of silica colloidal particles (n_s) and the refractive index of air (n_0):

$$n_{eff} = \sqrt{n_s^2 \times f + n_0^2 \times (1 - f)}. \qquad (2)$$

For ideal FCC PCs, $d = D$, $f = 0.74$. The calculated n_{eff} is 1.348 5. Inserting f and d_{eff} into the Eq. 1, $\lambda = 605$ nm is gained theoretically.

2.2　Plane Wave Expansive

Using PWE, the width of the photonic crystal band gap is calculated theoretically. Fig. 1. shows the PBG of the silica colloidal opal PCs. A pseudo gap is found in calculated result as shown in Fig. 1. The normalized frequency ($F = \omega a/2\pi c = a/\lambda$) of the PBG is ranged from 0.632 to 0.666. Using the

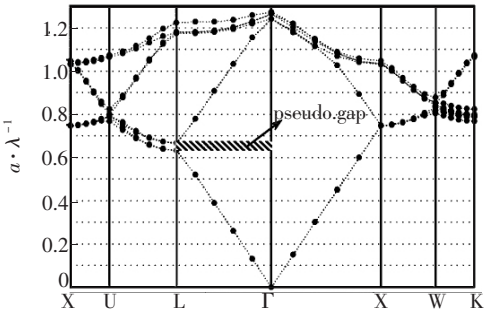

Fig. 1　The PBG of the silica colloidal opal PCs

equation $F = \omega a/2\pi c = a/\lambda$, the PBG ranged from 583 nm to 615 nm is gained.

3 Experimental Section

The silica colloidal particles is bought from Chinese university of petroleum (Beijing). The slides on which the opal PCs were fabricated were cleaned strictly according to the following process steps: Firstly, marinated in the chromic acid for not less than 24 h. Secondly, ultrasonic cleaned in acetone, ethanol and deionized water for ten minutes in sequence. The end, dried on the hot plate for several minutes. The colloidal suspension was diluted to 1% by ethanol. Vertical deposition was used to fabricate the opal PCs in room temperature for several days until the solution evaporated completely. Finally, the opals PCs samples were annealed under 150, 300, 450 ℃ respectively. The samples were characterized with HITACHI S-4800 scanning electron microscopy and UV3101PC UV-VIS-NIR scanning spectrophotometer.

4 Results and Discussion

4.1 The SEM Images of The Colloidal PCs

The SEM images of the opal PCs samples are shown in Fig. 2. In some region of the colloidal photonic crystals, both (111) and (100) orientation are observed on the same samples, as shown in Fig. 2(a). It is still unclear why (100) orientation forms, although the thermodynamic stability of the (111) orientation is stronger than that of the (100) orientation [31]. We believe that the temperature fluctuation and the shock of the samples during the progress are important reasons. The (100) orientation in the samples influences the optical properties of the colloidal PCs. Because there is no barrier exists in the (100) domains for the whole wave band when electromagnetic wave incidents on the samples. In most region of the PCs, the (111) orientation occupies dominant. The thickness of the colloidal PCs is about 16 μm, which means the colloidal particles are deposited for several hundreds layers, as shown in Fig. 2(b). Some of the line-defects, point-defects and dislocations are observed in the SEM images of the samples as shown in the Fig. 2(c). Since the experimental conditions are impossible to be controlled perfectly, it is difficult to avoid all the structural defects. The factors such as the fluctuation of the temperature and humidity, the vibration of the samples during the growth of the PCs influence the

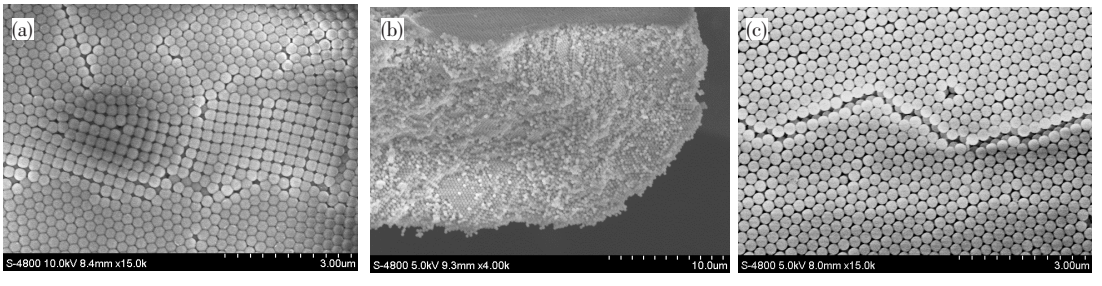

Fig. 2 SEM images of the PCs, (a) the (111) and (100) orientation in the PCs; (b) the thickness of the PCs; (c) the defects in the PCs.

quality of the opal PCs.

The shrink and deformation of the particles were observed. After annealed at 450 ℃, the diameter of colloidal particles decreased from 275 nm to 250 nm approximately, as shown in Fig. 3. The deformation of the particles is found not only in the annealed PCs, but also in the PCs fabricated without any heat treatment, as shown in Fig. 4. On the surface of the (111), the particle is compressed to nearly hexagon as shown in Fig. 4(a) and Fig. 4(b). Fig. 4(c) indicates that the deformation was found not only on the surface of the PCs, but also in the crack position. Therefore, we can conclude that the compression comes from all the orientation of the PCs, and the particles deform omnidirectionally. And also, the deformation phenomenon is observed in some other researchers' works, though the samples without annealing in their works [29-30]. The deformation of the

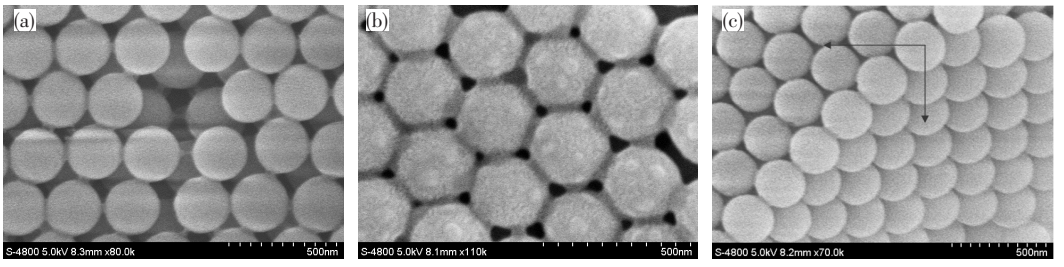

Fig. 3　The shrink of the particles annealed in 450 ℃

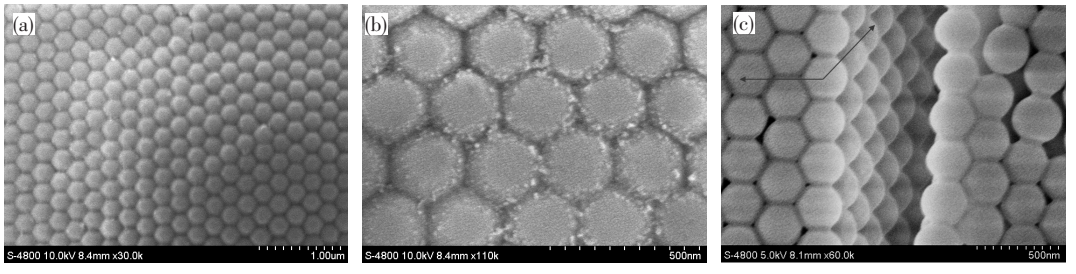

Fig. 4　The deformation of the particles: (a), (b) the deformation of the particles in the (111) orientation; (c) the deformation of the particles in the crack position.

particles comes from the internal stress, which makes the particles arrange closely. The deformation enhances the mechanical strength and density of the colloidal PCs greatly, which makes it possible to fabricate photonic crystal optical devices using the colloidal PCs. For example, wet etching is usually used in the fabrication of the photonic crystal devices, the deformation can reduce the lateral erosion in wet etching during the fabrication of the photonic crystal devices owing to the close arrangement of the particles.

Table 1　The optical properties of the samples

Annealing temperature/℃	PBG/nm	Width of PBG/nm	Central wavelength/nm	Absorption
Non-annealing	575 ~ 613.5	38.5	595	0.279 2
150	564.5 ~ 600	35.5	580	0.618 5
300	561 ~ 598	37	576.5	0.705 9
400	560.5 ~ 588.5	28	572.5	0.734 2
Theoretical	583 ~ 615	32	605	–

The optical properties of opal PCs samples were measured using the UV3101PC UV-VIS-NIR scanning spectrophotometer. Fig. 5 presents the absorption rate of the opal PCs in visible waveband. Upon increasing the annealing temperature, the width of the PBG decreases from 38.5 nm to 28 nm, and a blue shift of the central wavelength from 595 nm to 572.5 nm is observed. At the same time, the absorption rate enhances from 0.279 2 to 0.734 2. The optical properties are shown in Table 1.

Compared the test results of opal PCs samples without annealing to the PBG calculated in theoretical, the width of PBG of samples broadens for several nanometers. The PBGs of opal OPs overlap together due to silica particles with different diameters. these overlaps broaden the width of the PBG. The broadening

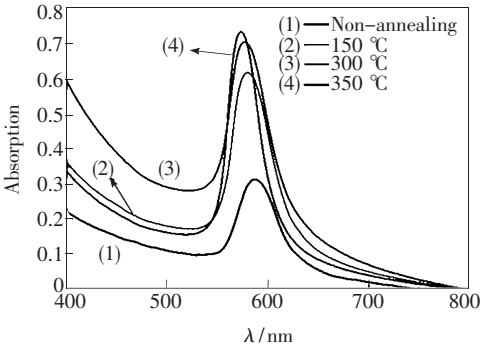

Fig. 5　The absorption rate of the opal PCs in visible waveband

degree is determined by the uniformity of the particle diameters.

From Table 1, it could be seen that the central wavelength of opal PCs sample blue shift to 572.5 nm after annealed in 450 ℃. The width of the PBG decreases to 28 nm. The blue shift and the reduction of the width of the PBG come form the shrink and the deformation of the particles. Obviously, there are difference between experimental results and calculated results by sphere model. In order to explain the phenomenon above, the theoretical model is amended.

4.2 The Amendment of The Theoretical Model

After annealing, the diameter of the particles shrank from 275 nm to 250 nm. The volume fraction is declined from 0.74 to 0.556. The effective refractive index is $n_{\text{eff}} = 1.27$ calculated through Eq. 2. The shrink of the particles dose not change the interval of the particles and the lattice structure. the spacing of (111) dominions is still $d_{\text{nkl}} = 0.816d$. Inserts the above parameters into Eq. 1, the central wavelength of the PBG is calculated about 570 nm finally. The width of the PBG is calculated through PWE. The normalized frequency of the PBG is ranged from 0.677 1 to 0.724 9. The wavelength of the PBG is calculated from 536 nm to 574 nm approximately through $F = \omega a/2\pi c = a/\lambda$.

Because of the deformation of the particles illustrated in Fig. 4, the silica colloidal particles compressed together closely by the internal stress, which leads to the deformation of the particles from sphere to dodecahedron as shown in Fig. 6(a). At the same time, the volume of the particles decreased with the deformation of the particles , which leads to the increasing of the filling rate. The change of the filling rate is the most important reason for the blue shift of the PBG and the decrease of the width of the PBG when increasing the annealing temperature.

In (111) orientation, the cross section of the particles changes form circle to hexagon as shown in Fig. 6(b) , which leads to the change of the radius . The parameters change as the deformation of the colloidal particles, as is shown in Table 2.

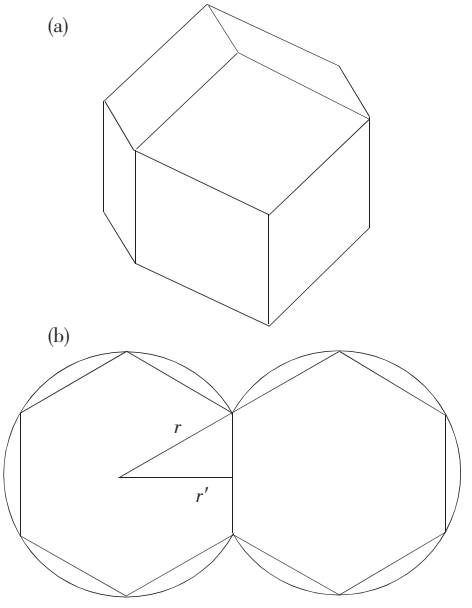

Fig. 6 The deformation of the colloidal particles, (a) the particles deformed from sphere to dodecahedron; (b) in the (111) orientation, the cross section of the particles is compressed from circle to hexagon.

Table 2 The changes of the parameters

	r/nm	D/nm	a/nm
Ex-deformation	137.5	275	388.85
Deformation	119.08	238.15	336.76

The central wavelength can be calculated through Eq. 1 and Eq. 2, For FCC structure, the volume fraction is defined as the volume of the spheres v_a divided by the volume of the primitive cell ν_{cell}:

$$f = \frac{v_a}{\nu_{\text{cell}}}, \tag{3}$$

After the annealing of opal PCs samples, the spheres are compressed to dodecahedrons, the volumes of the dodecahedrons ν'_a replace the volumes of the spheres ν_a. Because of the deformation of the spheres, ν'_a is smaller than ν_a. The different value is the volume of the twelve spherical segments ν_s:

$$\nu'_a = \nu_{\text{spheres}} - \nu_s, \tag{4}$$

The v_s is given by:

$$v_s = 6\pi h^2 \times \left(r - \frac{h}{3}\right), \tag{5}$$

where h is the height of the spherical segment, $h = \left(1 - \frac{\sqrt{3}}{2}\right)r$.

Inserting Eq. 4 and Eq. 5 into Eq. 3, $f = 0.963\ 6$ is obtained. Inserting $f = 0.963\ 6$ into Eq. 2, $n_{\text{eff}} = 1.436\ 1$ is obtained. The spacing of the (111) domains $d_{\text{nkl}} = 0.816d$, as the deformation of the spheres, d is the spacing of the adjacent dodecahedrons which is $\sqrt{3}r = 238.15$ nm here. So inserting the results above into Eq. 1, the calculating central wavelength is 558 nm.

Using the PWE, the width of the PBG is gained. A pseudo gap is found as shown in Fig. 7. The normalized frequency of the PBG is ranged from 0.598 99 to 0.608 48. We can gain the wavelength of the PBG ranged from 553 nm to 562 nm approximately, and the width of the PBG is 9 nm.

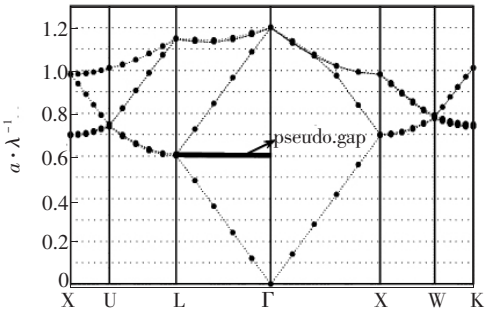

Fig. 7　The PBG of the deformed sample

For the central wavelength of the PBG, the results calculated with the amended model is 558 nm, which fits the measured results better than that calculated with sphere model. For the width of the PBG, the results calculated with new theoretical mode is much smaller than the measured results. The deviation between calculated results with the amended model and experimental results comes from the assumption during establishing mode. In the amended model, we hypothesize that the particles were compressed from spheres to dodecahedrons. In practical, many of the particles are compress to nonstandard dodecahedrons. In the nonstandard dodecahedrons, some surfaces are spherical surfaces yet, which means that the degree of the deformation is lower than predicated. As a response, the filling rate f is smaller than predicated too. Despite this, the amendment of the theoretical model provides a much better prediction before the experiment.

5　Conclusion

The silica colloidal PCs were fabricated and annealed. The shrink and deformation of the colloidal particles were observed. Upon increasing the annealing temperature, the samples showed a blue shift of the center wavelength of PBG for 22.5 nm, and the width of the PBG decrease for 10.5 nm. The optical influence of the deformation was discussed quantitatively, and the theoretical model was amended according to experimental results. The central wavelength of the PBG calculated with the amended model was 558 nm, which fit the experimental results much better than that calculated with sphere model. The deformation of the particles makes it available to fabricate 3D photonic crystal device with artificial opal PCs. The new model makes the more precise theoretical calculation possible, which provides convenience for the growth and application of the colloidal photonic crystals.

References:

[1] Yablonovitch E. Inhibited spontaneous emission in solid-state physics and electronics [J]. *Phys. Rev. Lett.*, 1987, **58**(20): 2059-2062.

[2] John S. Strong localization of photons in certain disordered dielectric superlattices [J]. *Phys. Rev. Lett.*, 1987, **58**(23): 2486-2489.

[3] Hu Xiaoyong, Jiang Ping, Ding Chengyuan, *et al*. Picosecond and low-power all-optical switching based on organic photonic band gap microcavity [J]. *Nature Photonics*, 2008, **2**(3): 185-189.

[4] Zhao H W, Zhang X Y, Yuan B, *et al*. Research on some new mechanisms of slow light and its applications [J]. *Optics and Precesion Enginerring* (光学 精密工程), 2009, **17**(2): 237-245 (in Chinese).

[5] Dowling J P, Scalora M, Bloemer M J, *et al*. The photonic band edge laser: A new approach to gain enhancement [J]. *J. Appl. Phys.*, 1994, **75**(4): 1896-1899.

[6] Shih M H, Kim W J, Kuang W, *et al*. Experimental characterization of the reflectance of 60° waveguide bend in photonic

crystal waveguide [J]. *Appl. Phys. Lett.*, 2005, **86**(19): 191104-1-3.

[7] Brown E R, Parker C D. Yabnolovitch E. Radiation properties of a planar antenna on photonic crystal substrate [J]. *J. Opt. Soc. Am.* B, 1993, **10**(2): 404-407.

[8] Wang C C, Chen L W. Tunable two-dimensional photonic crystal couplers made of dielectric elastomer inclusions [J]. *Appl. Opt.*, 2010, **49**(18): 3452-3457.

[9] Qiu M, Jaskorzynska B. Design of a channel drop filter in a two-dimensional triangular photonic crystal [J]. *Appl. Phys. Lett.*, 2003, **83**(10): 10764-1-3.

[10] Tada T, Poborchii V V, Kanayama T. Channel waveguides fabricated in 2D photonic crystals of Si nanopillars [J]. *Microelectron. Eng.*, 2002, **63**(1): 259-265.

[11] Charlton M D B, Zoorob M E, Parker G J, *et al.* Experimental investigation of photonic crystal waveguide devices and line-defect waveguide bends [J]. *Mat. Sci. Eng.* B, 2000, **74**(1): 17-24.

[12] Han S Z, Tian J, Feng S, *et al.* Fabrication of straight waveguide in two-dimensional photonic crystal slab and its light propagation characteristics [J]. *Acta Phys. Sin.* (物理学报), 2005, **54**(12): 5659-5662 (in Chinese).

[13] Wang J C, Rong W B, Li X X, *et al.* Fabrication process analysis fro nano-positioning stage based on silicon bulk micromachining [J]. *Optics and Precesion Enginerring* (光学 精密工程), 2008, **16**(4): 636-641.

[14] McPhail D. Optical tuning of three-dimensional photonic crystals fabricated by femtosecond direct writing [J]. *Appl. Phys. Lett.*, 2005, **87**(9): 091117-1-3.

[15] Miklyaev Y V, Meisei D C, Blanco A, *et al.* Three-dimensional face-centered-cubic photonic crystal templates by laser holography: fabrication, optical characterization, and band-structure calculations [J]. *Appl. Phys. Lett.*, 2003, **82**(8): 1284-1286.

[16] Jiang P, Bertone J F, Shuang K, *et al.* Single-crystal colloidal multilayers of controlled thickness [J]. *Chem Mater.*, 1999, **11**(8): 2132-2140.

[17] Chang Y C, Wu H W, Chen H L, *et al.* Two-dimensional inverse opal ZnO nanorod networks with photonic band gap [J]. *J. Phys. Chem.* C, 2009, **113**(33): 14778-14782.

[18] Wang W, Gu B H, Liang L Y, *et al.* Fabrication of two- and three-dimensional silica nanocolloidal particle arrays [J]. *J. Phys. Chem.* B, 2003, **107**(15): 3400-3404.

[19] Wang W, Gu B H, Liang L Y, *et al.* Fabrication of two- and three-dimensional silica nanocolloidal particle arrays [J]. *J. Phys. Chem.* B, 2003, **107**(15): 3400-3404.

[20] Rugge A, Park J S, Gordon R G. *et al.* Tantalum(V) nitride inverse opals as photonic structures for visible wavelengths [J]. *J. Phys. Chem.* B, 2005, **109**(9): 3764-3771.

[21] Zhou Z C, Zhao X S. Flow-controlled vertical deposition method for the fabrication of photonic crystals [J]. *Langumir*, 2004, **20**(4): 1524-1526.

[22] Ye Y H, LeBlanc F, Hahcé A, *et al.* Self-assembling three-dimensional colloidal photonic crystal structure with high crystalline quality [J]. *Appl. Phys. Lett.*, 2001, **78**(1): 52-54.

[23] Holgado M, Garcia-Santamaria F, Blanco A, *et al.* Electrophoretic deposition to control artificial opal growth [J]. *Langmuir*, 1999, **15**(14): 4701-4704.

[24] Pozaas R, Mihi A, Ocana M, *et al.* Building nanocrystalline planar defects within self-assembled photonic crystals by spin-coating [J]. *Adv. Mater.*, 2006, **18**(9): 1183-1187.

[25] Vlasov Y A, Bo X Z, Sturm J C, *et al.* On-chip material assembly of silicon photonic bandgap crystals [J]. *Nature*, 2001, **414**(6861): 289-293.

[26] Yan Q F, Nukala P, Chiang Y, *et al.* Three-dimensional metallic opals fabricated by double templating [J]. *Thin Solid Films*, 2009, **517**(17): 5166-5171.

[27] Zheng Z Y, Gao K Y, Luo Y H, *et al.* Rapidly infrared-assisted cooperatively self-assembled highly ordered multiscale porous materials [J]. *J. Am. Chem. Soc.*, 2008, **130**(30): 9785-9789.

[28] Sun Z Q, Chen X, Zhang J H, *et al.* Nonspherical colloidal crystals fabricated by the thermal pressing of colloidal crystal chips [J]. *Langmuir*, 2005, **21**(20): 8987-8991.

[29] Li J, Xue L J, Wang Z. *et al.* Colloidal photonic crystals with a graded lattice-constant distribution [J]. *Colloid Polym. Sci.*, 2007, **285**(9): 1037-1041.

[30] Sinitskii A S, Knot'ko A V, Tretyakov Y D. Silica photonic crystals: synthesis and optical properties [J]. *Solid State Ionics*, 2004, **172**(1-4): 477-479.

[31] Deubel M, Freymann G V, Wegener M. *et al*. Direct laser writing of three-dimensional photonic-crystal templates for telecommunications [J]. *Nature Mater*, 2004, **3**(7): 444-447.

二氧化硅蛋白石光子晶体中粒子重构对光学性质的影响

崔乃迪[1,2]，梁静秋[1]，梁中翥[1]，周建伟[1,2]，王维彪[1*]

(1. 中国科学院长春光学精密机械与物理研究所 应用光学国家重点实验室，吉林 长春　130033;
2. 中国科学院 研究生院，北京　100039)

摘要： 使用自组装法制备了蛋白石结构二氧化硅纳米球三维光子晶体，并对样品在 150，300，450 ℃温度下进行了热处理。随热处理温度的升高，光子晶体禁带中心波长出现 22.5 nm 的蓝移，且禁带宽度变窄。对于在 450 ℃热处理的样品，其测量的禁带中心波长为 572.5 nm，与理论计算结果有较大差异。引起样品光学特性变化的原因是热处理后二氧化硅球体形变和重构。进一步分析了小球形变对样品光学特性的影响，根据实验结果，修正了计算模型。利用修正后的模型计算样品禁带中心波长为 558nm，和实验结果符合良好。

关　键　词： 光子晶体；自组装；光子禁带
中图分类号： O431.1　　**PACS:** 42.70.Qs　　**PACC:** 4270Q; 4225B　　**文献标识码：** A
文章编号： 1000-7032(2011)06-0542-08

收稿日期： 2011-04-25；**修订日期：** 2011-05-15
基金项目： 国家自然科学基金(60877031)资助项目
作者简介： 崔乃迪(1983－)，男，黑龙江双鸭山人，主要从事光子晶体光电器件设计及制备方面的研究。E-mail: cuinaidi@163.com
*：通讯联系人；E-mail: wangwbt@126.com